679

Dev Genes Evol (2007) 217:105–118
DOI 10.1007/s00427-006-0118-z

ORIGINAL ARTICLE

Brefeldin A or monensin inhibits the 3D organizer in gastropod, polyplacophoran, and scaphopod molluscs

Eric E. Gonzales · Maurijn van der Zee · Wim J. A. G. Dictus · Jo van den Biggelaar

Received: 18 April 2006 / Accepted: 17 October 2006 / Published online: 22 November 2006

Abstract In molluscs, the 3D vegetal blastomere acts as a developmental signaling center, or organizer, and is required to establish bilateral symmetry in the embryo. 3D is similar to organizing centers in other metazoans, but detailed comparisons are difficult, in part because its organizing function is poorly understood. To elucidate 3D function in a standardized fashion, we used monensin and brefeldin A (BFA) to rapidly and reversibly interfere with protein processing and secretion, thereby inhibiting the signaling interactions that underlie its specification and patterning. In the gastropods, *Patella vulgata* and *Lymnaea stagnalis*, the polyplacophoran, *Mopalia muscosa*, and the scaphopod, *Antalis entalis*, treatments initiated before the organizer-dependent onset of bilateral cleavage resulted in radialization of subsequent development. In radialized *P. vulgata*, *L. stagnalis*, and *M. muscosa*, organizer specification was blocked, and embryos failed to make the transition to bilateral cleavage. In all four species, the subsequent body plan was radially symmetric and was similarly organized about a novel aboral–oral axis. Our results demonstrate that brefeldin A (BFA) and monensin can be used to inhibit 3D's organizing function in a comparative fashion and that, at least in *M. muscosa*, the organizer-dependent developmental architecture of the embryo predicts subsequent patterns of morphogenetic movements in gastrulation and, ultimately, the layout of the adult body plan.

Keywords Developmental signaling center · Monensin · Brefeldin A · Spiral cleavage · 3D organizer

Communicated by D.A. Weisblat

E. E. Gonzales · M. van der Zee · W. J. A. G. Dictus · J. van den Biggelaar
Department of Developmental Biology, University of Utrecht, Padualaan 8,
3584 CH Utrecht, The Netherlands

E. E. Gonzales
Friday Harbor Laboratories, University of Washington,
620 University Road,
Friday Harbor, WA 98250, USA

E. E. Gonzales
Smithsonian Marine Station, Smithsonian Institution,
701 Seaway Drive,
Fort Pierce, FL 34949, USA

E. E. Gonzales (✉)
Center for Integrative Genomics,
University of California at Berkeley,
142 Life Sciences Addition,
Berkeley, CA 94720, USA
e-mail: eegonzales@berkeley.edu

Introduction

Development in many lophotrochozoan phyla is characterized by spiral cleavage, a D-quadrant-dependent transition to bilateral cleavage, and gastrulation in a trochophore larva. Spiral cleavage occurs in molluscs, annelids, polyclad flatworms, nemerteans, and other phyla (Halanych 2004; Wilson 1898). Its stereotypic patterns of division and determinant segregation create a highly organized developmental architecture that is radially symmetric about and polarized along the animal–vegetal axis (Lambert and Nagy 2002; Sweet 1998). In spiral-cleaving embryos, each cell can be uniquely identified using a nomenclature of quadrants (A, B, C, D) and quartets (1, 2, 3, 4; Wilson 1892), and each makes a stereotypic contribution to the adult, with some cell lineage contributions conserved across phyla (Wilson 1898). A transition from spiral to bilateral cleavage occurs before the onset of gastrulation (Wilson 1892) and requires patterning by a signaling center that is

localized to the vegetal D-quadrant (Clement 1962; Crampton 1896; Wilson 1904). Patterning by this organizing center establishes a secondary axis in the embryo and results in a developmental architecture that, as shown by patterns of cell division (van den Biggelaar 1977), lineage contribution (Dictus and Damen 1997), and gene expression (Lartillot et al. 2002b) in gastropod molluscs, is bilaterally symmetric and polarized along two perpendicular axes, the primary animal–vegetal axis and a secondary organizer-dependent axis. The secondary axis is commonly referred to as either the anterior–posterior axis, with D-quadrant as posterior, or the dorsal–ventral axis, with D-quadrant as dorsal; however, many blastomeres at the time of patterning make lineage contributions that are neither structure- nor axis-specific (Dictus and Damen 1997). Gastrulation begins shortly after the transition to bilateral cleavage and is completed in the trochophore larva, which is composed of larval swimming structures and morphogenetic domains that give rise to adult anlagen. The trochophore typically transitions to a taxon-specific secondary larval stage, e.g., the gastropod veliger, which differentiates adult structures and undergoes settlement and metamorphosis to produce the juvenile and later adult.

Developmental organizers are signaling centers that pattern the cells or region around them. They are often required for proper establishment of the body plan in metazoan development, typically localized to the vegetal pole and patterning the early embryo through gastrulation in diverse phyla (Martindale 2005). In molluscs, annelids, nemerteans, and perhaps other spiral-cleaving lophotrochozoans, a developmental organizer in the vegetal D-quadrant is required for the transition to bilateral cleavage and later establishment of the body plan. This was first demonstrated in polar-lobe-forming molluscs and annelids, where experimentally induced loss or duplication of the vegetal D-quadrant results in the subsequent loss or duplication of bilateral cleavage and of the primary body axis, i.e., radialization or twinning of the embryo and body plan (Clement 1952; Crampton 1896; Tyler 1930; Wilson 1904). In molluscs, this organizer is the 3D blastomere, which acts as a transient signaling center that patterns the embryo sometime after the onset of the fifth cleavage, but is not maintained in gastrulation (Cather and Verdonk 1979; Clement 1962). As mentioned, 3D patterning establishes a secondary axis that is reflected in patterns of cleavage, cell lineage, and gene expression. The nature of this axis and the molecular mechanisms surrounding 3D's organizing function remain poorly understood, but a number of genes characteristic of organizing centers in other phyla are expressed in midline lineages dependent upon 3D patterning. This suggests that the organizer function of 3D reflects a potentially ancient feature of metazoan development and evolution (Lartillot et al. 2002a,b).

Organizer specification is different in species undergoing equal versus unequal cleavage (Freeman and Lundelius 1992; Henry et al. 2006). In unequal-cleaving and polar-lobe-forming species, specification is through the segregation of the maternal determinants to a single vegetal macromere during early divisions. How 3D's organizing activity is later induced varies between unequal-cleaving species. For instance, animal–vegetal interactions are required in the slipper snail *Crepidulafornicata* (Henry et al. 2006) but are not required in the mudsnail *Ilyanassa obsoleta* (Clement 1967). In contrast, in equal-cleaving gastropods, such as *Patella vulgata* and *Lymnaea stagnalis*, the vegetal region and associated maternal determinants are not segregated to a single lineage, and all four vegetal macromeres remain competent to act as 3D through the onset of the fifth cleavage (Arnolds et al. 1983). In these embryos, 3D specification and induction requires selection of one from the four macromeres and is achieved stochastically through inductive interactions between the animal and vegetal poles (van den Biggelaar 1977; van den Biggelaar and Guerrier 1979). In *P. vulgata*, specification is initiated by extension of the animal $1q^{11}$ and vegetal 3Q quartets into the cleavage cavity during the 32-cell resting stage, where they establish contact (van den Biggelaar 1977). Inhibition of contact, e.g., by using monensin as a general block to cell signaling and secretion, results in a failure to specify 3D, with radialization of the embryo and body plan (Arnolds et al. 1983; Kuhtreiber et al. 1988; van den Biggelaar and Guerrier 1979), similar to lobeless or ablated unequal-cleaving embryos. Despite differences in specification, equal- and unequal-cleaving embryos activate mitogen-activated protein kinase (MAPK) in 3D around the time of patterning and are similarly radialized by treatment with U0126, an inhibitor of MAPK activation (Lambert and Nagy 2001, 2003; Lartillot et al. 2002b), suggesting that the different systems converge downstream of specification.

A comparative understanding of the 3D organizer in molluscs is critical to understanding the evolution and development of body-plan disparity and diversity in molluscs, spiral-cleaving lophotrochozoans, and metazoans in general. Although the 3D organizer has been demonstrated in gastropod, polyplacophoran, and scaphopod classes, direct comparisons are problematic due to differences in the experimental techniques of different studies. To comparatively characterize 3D in a more standardized fashion, we used two general inhibitors of protein processing and secretion, monensin and BFA (Dinter and Berger 1998; Mayer 2003; Mollenhauer et al. 1990), to test for the presence and function of 3D patterning in the equal-cleaving gastropods, *P. vulgata* and *L. stagnalis*, the equal-cleaving chiton, *Mopalia muscosa*, and the polar-lobe-forming scaphopod, *Antalis entalis*. We then documented the resulting radialized development in each,

focusing in particular on *M. muscosa*. Our results show that either one or both chemicals are effective tools for inhibiting 3D's organizing function in each species and that radialized larvae of each are similarly organized about a novel aboral–oral axis.

Materials and methods

Collection and culturing

Adult *P. vulgata* (Mollusca, Gastropoda; limpet) were collected intertidally at the Station Biologique de Roscoff in Roscoff, France in 1998. Adults were maintained and fertilizations made according to Kuhtreiber et al. (1988). Synchronously dividing embryos were selected at first and second cleavage, and synchronous embryos of multiple females were pooled after collection. Embryos and larvae were cultured in fresh seawater (FSW) with antibiotics (60 mg/l penicillin G and 50 mg/l streptomycin) and stirred at 18°C. Adult *L. stagnalis* (Mollusca, Gastropoda; snail) were collected in 1998 from the canals in Utrecht, The Netherlands. Adults were maintained and embryos collected according to Arnolds et al. (1983). Synchronous embryos from a single egg mass exhibiting normal development were used for each experiment. Adult *M. muscosa* (Mollusca, Polyplacophora; chiton) were collected intertidally on San Juan Island, Washington in 1997 and 1998. Individuals spawned spontaneously after collection, or after being starved for 3–4 days and given an alternating series of 10°C temperature shocks. Early development was highly synchronous, and embryos were cultured in FSW at ambient seatable temperatures (10–12°C). Adult *A. entalis* (Mollusca, Scaphopoda; tusk shell) were collected by dredging at the Station Biologique de Roscoff in Roscoff, France in 1998. Adults were maintained at room temperature in bowls containing their natural habitat of shell hash and kept under running seawater. Spawning was induced by isolating individual adults in a fingerbowl without habitat or running seawater. Embryos were incubated in FSW at room temperature (20°C) in fingerbowls. Early development was asynchronous by up to several hours between embryos.

Treatment with BFA and monensin

BFA and monensin are small organic molecules used as pharmacological tools to provide a rapid and reversible inhibition of protein processing and secretion in eukaryotes (Dinter and Berger 1998; Mayer 2003; Mollenhauer et al. 1990). Monensin inhibits 3D specification at specific timepoints in gastropod development (Kuhtreiber et al. 1988), and because the target and/or function of each chemical is highly conserved, both can be used to test for organizer presence and function in developmentally uncharacterized species, where genomic and molecular genetic tools are lacking.

One millimolar BFA (Sigma) and monensin (Sigma) stocks in ethanol were stored at −20°C. Working concentrations of 10 μM to 1 nM were prepared in FSW. Embryos were incubated at different concentrations for up to 3 h and then washed five times with FSW. To radialize development, embryos were incubated during the known or predicted period of 3D specification and patterning, beginning at the 32-cell onset in *P. vulgata* and *M. muscosa* and at the 24-cell onset in *L. stagnalis* and *A. entalis*. Identical treatments were also made either before and/or after specification and patterning in *P. vulgata*, *L. stagnalis*, and *M. muscosa*. Each treatment was surveyed on a dissecting microscope, and subsamples of 20–100 larvae were scored at higher magnifications. Control treatments of 0.1% ethanol had no observable effect on development in *P. vulgata*, *L. stagnalis*, and *M. muscosa*.

Embryonic and larval analysis

To assess cleavage patterns, embryos were fixed according to Kuhtreiber et al. (1988) every 20 to 30 min through early gastrulation in *M. muscosa* and *A. entalis* and at known developmental stages in *P. vulgata* and *L. stagnalis*. *P. vulgata*, *M. muscosa*, and *A. entalis* embryos were gallocyanin-stained and mounted (Kuhtreiber et al. 1988), and *L. stagnalis* embryos were silver-stained and mounted (Arnolds 1979). Developmental stages were documented using camera lucida or light photomicrographs. Camera lucida drawings were scanned and then traced using Adobe Photoshop and Illustrator. To assess larval morphology, larvae were photographed live or fixed and analyzed by scanning electron microscopy according to Kuhtreiber et al. (1988). To assess neural and muscle differentiation in *M. muscosa*, larvae were prepared for confocal analysis according to Wanninger and Haszprunar (2002). Cell boundaries and muscle were visualized by phalloidin (Molecular Probes) labeling of f-actin. Neural differentiation was characterized using anti-serotonin (Immunostar) and anti-FMRF-amide (Immunostar) primary antibodies and AlexaFluor fluorescent secondary antibodies (Invitrogen).

Results

BFA- and monensin-induced radialization in the gastropod *P. vulgata*

One micromolar monensin and BFA treatments beginning at the 32-cell stage and lasting 1–3 h resulted in nearly

100% radialized development of embryos and larvae (Fig. 1). In contrast, identical treatments initiated after the onset of bilateral cleavage at 56-cells had no observable effect on development (Fig. 1a). Thus, radialization was specific to the period of organizer specification and patterning. Treatments made at concentrations of 0.1 μM or less had no observable effect on development, whereas 10-μM treatments were lethal (Fig. 1b).

Organizer specification in normal development is initiated by extension and contact of the animal $1q^{11}$ and vegetal 3Q quartets during the 32-cell resting stage, resulting in centralization of a single vegetal macromere, 3D (Fig. 1c). Specification did not occur in BFA- and monensin-radialized embryos. The $1q^{11}$ and 3Q quartets failed to fully extend into the cleavage cavity, animal–vegetal contact was not established, and centralization of a single macromere did not occur (Fig. 1f). In normal development, the transition to bilateral cleavage can be used as a morphological proxy of 3D patterning and its establishment of a secondary developmental axis. This transition is first evident within the 3q quartet at the 56-cell stage when 3c and 3d divide bilaterally, whereas 3a and 3b divide spirally, and within the 3Q quartet at the 60-cell stage when 3A–3C asynchronously divide before 3D (Fig. 1d). The transition to bilateral cleavage did not occur in BFA- and monensin-radialized embryos; divisions within the 3q and 3Q quartets remained synchronous and spiral (Fig. 1g).

Larval trochophores differentiate an apical organ, characterized externally by a long apical tuft surrounded by shorter apical cilia, and prototroch (Fig. 1e). BFA- and

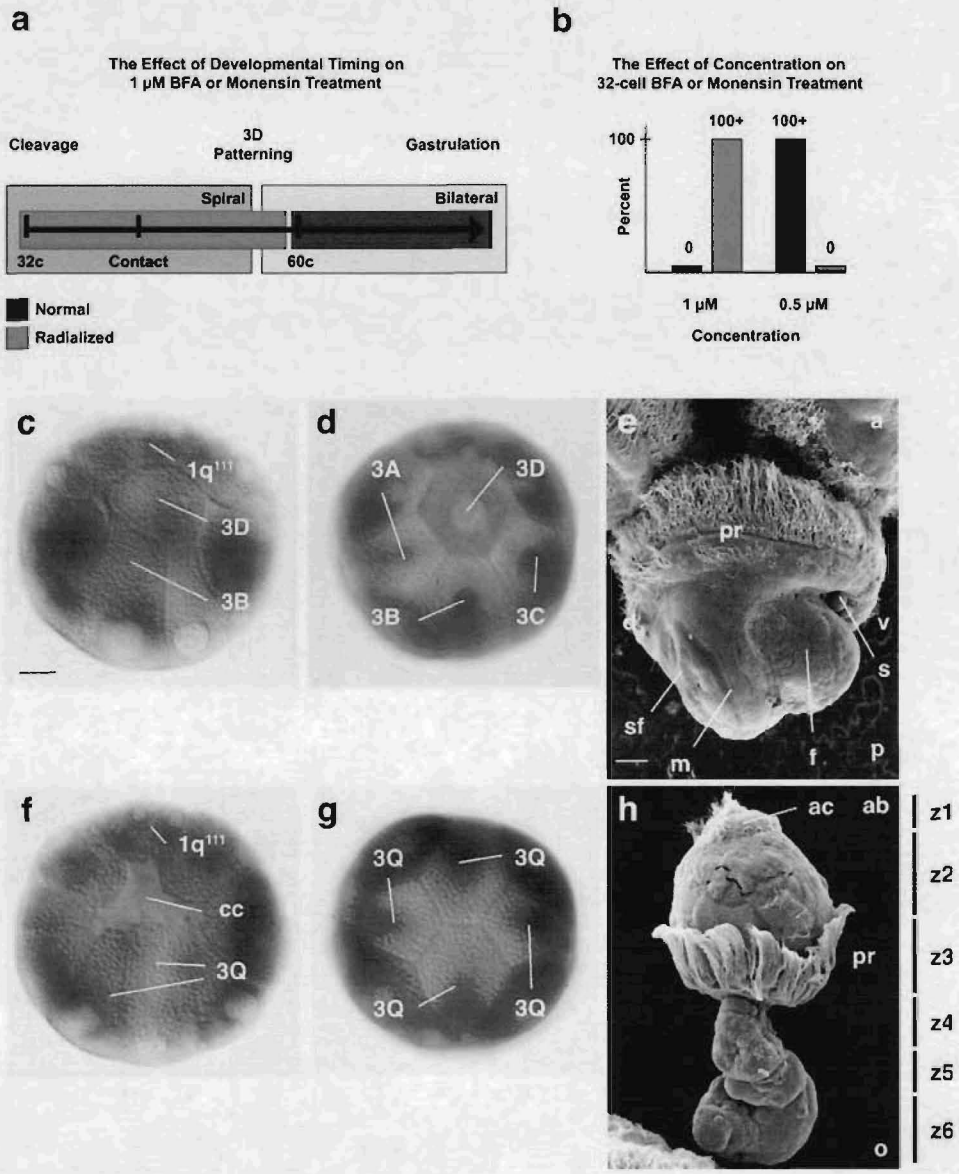

Fig. 1 BFA and monensin treatments in *P. vulgata* inhibit animal–vegetal contact, resulting in radialization of the embryo and body plan. **a** is a schematic showing the effects of developmental timing on 1 μM BFA or monensin treatments. **b** is a graph showing the effects of concentration on BFA or monensin treatments. **c–e** show normal 3D specification and patterning and the body plan. **c** shows 3D centralized and contacting the $1q^{11}$ quartet at the 56-cell stage (lateral). **d** shows 3A–3C dividing before 3D at the 60-cell stage (vegetal). **e** shows the body plan symmetrically organized about the anterior–posterior and dorsal–ventral axes at 24 h (lateral). **f–h** show identical stages in 1 μM BFA-radialized development. **f** shows the failure to centralize a single 3Q macromere at the 56-cell stage (lateral). **g** shows the synchronous division of 3Q at the 60-cell stage (vegetal). **h** shows the larval adult body plan radially organized about a novel aboral–oral axis at 24 h (lateral). **c**, **d**, **f**, and **g** are photomicrographs of gallocyanin-stained embryos; **e** and **h** are scanning electron micrographs. *a* Anterior, *ab* aboral, *ac* apical cilia, *cc* cleavage cavity, *d* dorsal, *f* foot, *m* mantle, *o* oral, *p* posterior, *pr* prototroch, *s* stomodeum, *sf* shell field, *v* ventral. Scale bar=20 μm

monensin-radialized trochophores lacked an apical tuft but differentiated an expanded field of apical cilia and a functional prototroch (Fig. 1h). In normal development, gastrulation is complete by 24 h, and the trochophore gives rise to the early veliger, with characteristic adult anlagen, including the shell field, mantle, foot, and stomodeum, symmetrically arranged about the anterior–posterior and dorsal–ventral axes (Fig. 1e). BFA- and monensin-radialized veligers retained the radial symmetry of the embryo and formed distinct rings of different cell types, or tissues, organized into radial zones along a novel aboral–oral axis (Fig. 1h). This axis paralleled the animal–vegetal axis but was distinct from it due to the internalization of vegetal lineages. The oral pole was defined by the site of gastrulation, which gives rise to the stomodeum during normal development, whereas the aboral pole lay opposite it. Zone 1 at the aboral pole consisted of an expanded field of apical cilia and zone 3 consisted of the prototroch. The remaining zones were distinct but could not be identified relative to normal development (Fig. 1h).

BFA-induced radialization in the gastropod *L. stagnalis*

Monensin treatments over a range of concentrations (10–0.5 μM), durations (up to 24 h), and developmental stages (beginning at the 1-cell and 24-cell stage) had no obvious effect on development (data not shown). In contrast, 16.5 μM BFA treatments initiated at the onset of the 24-cell stage and lasting for 3 h resulted in nearly 100% radialized development, including inhibition of 3D specification and loss of bilateral symmetry in the embryo and larval adult (Fig. 2a). Treatments at 33 μM were lethal, whereas 3.5-μM treatments had no effect (Fig. 2b). The 16.5-μM treatments, beginning either between the 1- and 8-cell stage and completed before the 24-cell stage or else 2 h after the transition to bilateral cleavage, had no observable effect on development (Fig. 1a), indicating that radialization was specific to the period of organizer specification and patterning.

Organizer specification in normal development is initiated by extension and contact of the animal $1q^1$, $1q^2$, and vegetal 3Q quartets during the 24-cell resting stage and results in centralization of a single vegetal macromere, 3D. In BFA-radialized embryos, 3D specification did not occur. The $1q^1$, $1q^2$, and 3Q quartets failed to fully extend into the cleavage cavity, animal–vegetal contact was not established, and centralization of a single macromere did not occur (data not shown). In normal development, RNA-rich vesicles, known as ectosomes, migrate away from the vegetal cortex in all four 3Q macromeres and, after 3D centralization, are dispersed in 3D, but condensed in 3A–3C. The transition to bilateral cleavage occurs shortly and is first evident within the 3Q quartet when 3D asynchronously divides before 3A–3C and within the 3q quartet when 3c and 3d divide bilaterally and 3a and 3b divide later and spirally (Fig. 2c). In radialized embryos, ectosome migration was similar to controls. However, ectosome dispersal did not occur, and the ectosomes became condensed in all four macromeres (data not shown). Subsequently, the transition to bilateral cleavage did not occur, and divisions within the 3q and 3Q quartets remained synchronous and spiral (Fig. 2f). In control embryos, early trochophores undergo morphogenetic movements in gastrulation, as the blastopore migrates to a more anterior ventral position, where it gives rise to the stomodeum (Fig. 2d). In 40-h veligers, adult anlagen of the head and trunk are symmetrically arranged about the anterior–posterior and dorsal–ventral axes as is the anterior ventral stomodeum (Fig. 2e). In contrast, radialized trochophores invaginated the vegetal pole during gastrulation but gave rise to radially symmetric and hydropic larvae that were organized about a novel aboral–oral axis (Fig. 2f,g). Aboral lineages formed a swollen vesicle, and oral lineages formed a compacted mass with internalized cells, presumably ectoderm with internalized vegetal endodermal and/or mesodermal lineages (Fig. 2h,i). Similar to radialized *P. vulgata*, the aboral–oral axis paralleled the animal–vegetal axis, but was distinct from it due to gastrulation. In later stages, discrete zones formed along the aboral–oral axis, and the zone between the swollen aboral and compacted oral regions became constricted, giving the larvae a characteristic dumbbell-shaped appearance (Fig. 2h,i). Radialized veligers maintained this initial condition into later stages, long after the overt differentiation of adult structures in controls (data not shown). After several days, it was common for radial larvae to break in half at the aboral–oral constriction point and die (data not shown).

Monensin-induced radialization in the polyplacophoran *M. muscosa*

One micromolar monensin treatments initiated at the 32-cell stage and lasting 3 h resulted in nearly 100% radialized development (Fig. 3a), including inhibition of 3D specification and the subsequent loss of bilateral symmetry in the embryo and larval adult (Figs. 3, 4, 5, 6, and 7). Identical treatments made after the onset of bilateral cleavage resulted in relatively normal development (Fig. 3a), indicating that radialization was specific to the period of organizer specification and patterning. Lower concentrations (0.5 μM) resulted in normal development (Fig. 3b).

Although largely undescribed, *M. muscosa* development is similar to that of other chitons (Heath 1899; van den Biggelaar 1996). At the 36-cell stage, a single non-cross-furrow macromere, designated 3D based on centralization and patterns of bilateral cleavage, initiates organizer specification and extends into the cleavage cavity, whereas

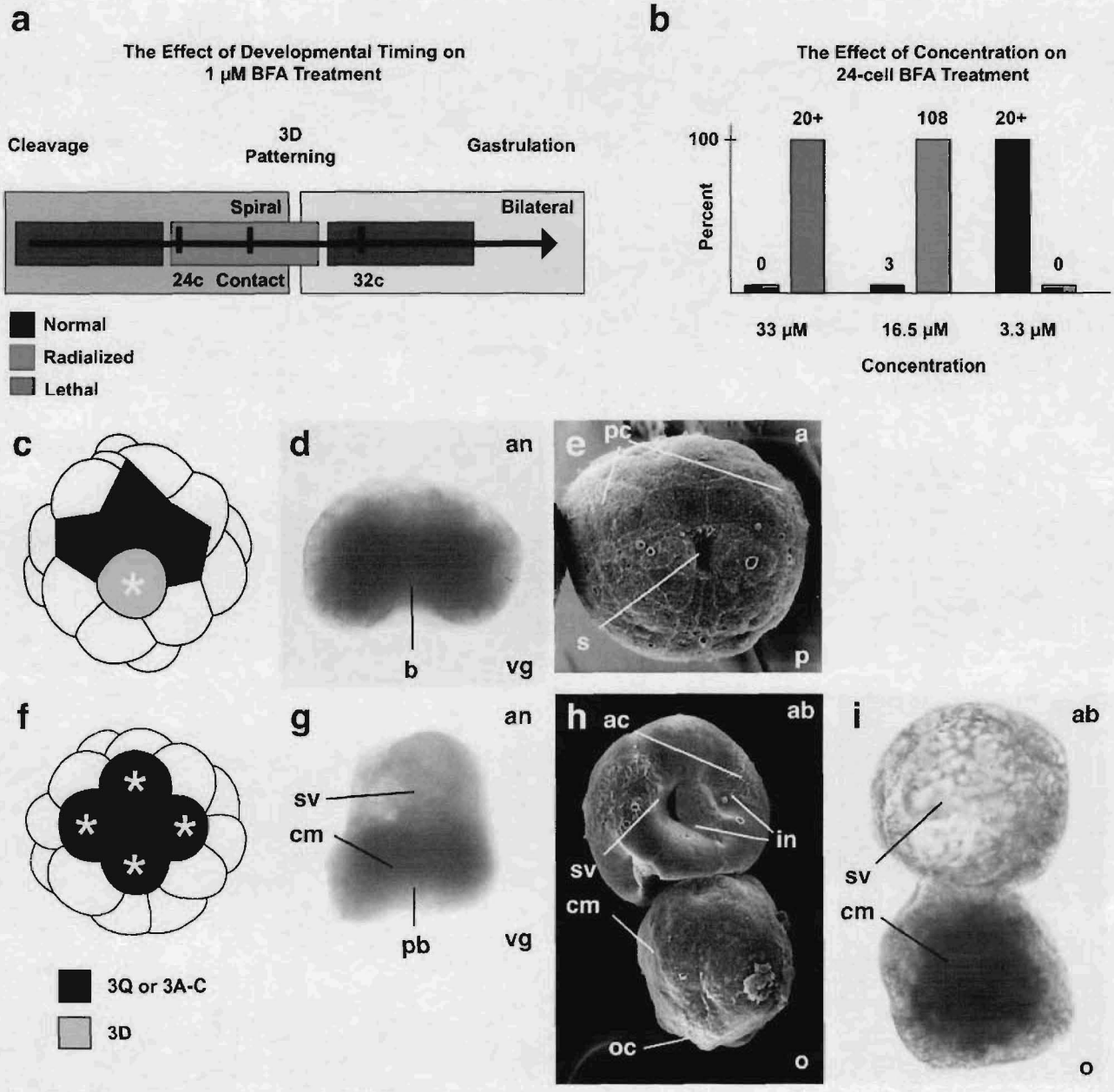

Fig. 2 BFA treatment in *L. stagnalis* inhibits animal–vegetal contact, resulting in radialization of the embryo and body plan. **a** is a schematic showing the effects of developmental timing on 16.5 μM BFA treatment. **b** is a graph showing the effects of concentration on BFA treatment. **c**–**e** show normal 3D specification and patterning and the body plan. **c** shows 3D dividing before blastomeres 3A–3C at the 24-cell stage (vegetal). **d** shows the invaginating blastopore at 37 h (lateral). **e** shows the body plan anlagen symmetrically organized about the anterior–posterior and dorsal–ventral axes at 42 h (ventral). **f**–**i** show identical stages in 16.5 μM BFA-radialized development. **f** shows the 3Q quartet dividing synchronously at the 24-cell stage (vegetal). **g** shows the invaginating blastopore at 37 h (lateral). **h**, **i** show the body plan radially organized about a novel aboral–oral axis at 42 h (lateral). **c** and **f** are camera lucida drawings; **d**, **g**, and **i** are live photomicrographs; **e** and **h** are scanning electron micrographs. *a* Anterior, *ab* aboral, *ac* aboral cilia, *an* animal, *b* blastopore, *cm* compacted mass, *in* aboral indentation, *o* oral, *oc* oral cilia, *p* posterior, *pb* potential blastopore, *pc* prototroch cilia, *s* stomodeum, *sv* swollen vesicle, *vg* vegetal

3A–3C remain at the surface. 3D establishes contact with all eight $1q^{11}$ and $1q^{12}$ micromeres by the 44-cell stage and occupies a centralized position within the cleavage cavity (Fig. 3c). Specification was inhibited in radialized embryos, as none of the 3Q macromeres extended into the cleavage cavity and animal–vegetal contact was not established (Fig. 3f). In controls, bilateral cleavage is initiated after centralization, with $2d^2$ producing a large $2d^{21}$ and small $2d^{22}$, whereas $2a^2$–$2c^2$ produce small $2a^{21}$–$2c^{21}$ but large $2a^{22}$–$2c^{22}$. At the 60-cell stage, $2a^{22}$–$2c^{22}$ extend either

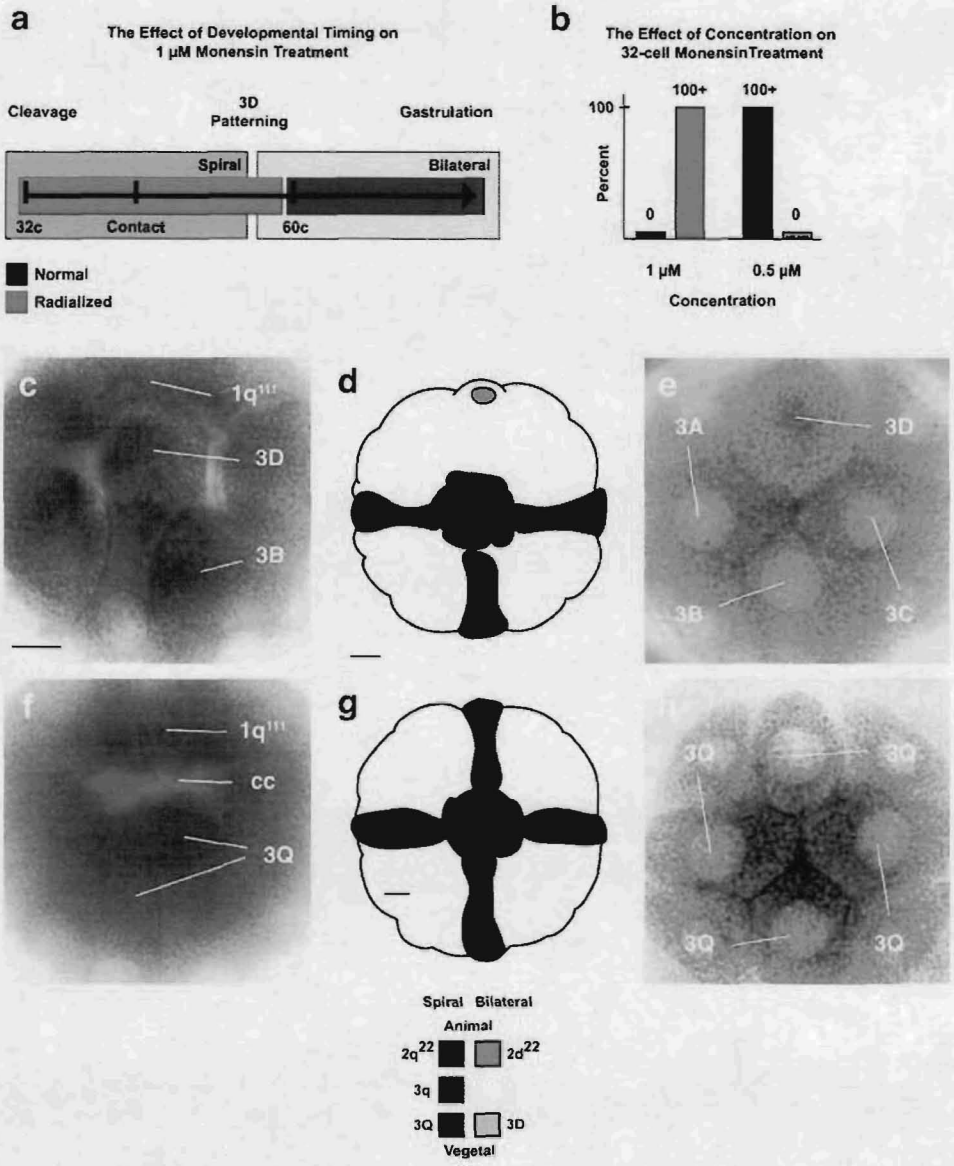

Fig. 3 Monensin treatment in *M. muscosa* inhibits animal–vegetal contact, resulting in the loss of bilateral cleavage in the embryo. **a** is a schematic showing the effects of developmental timing on 1 μM monensin treatments. **b** is a graph showing the effects of concentration on monensin treatments initiated at the 32-cell stage. **c**–**e** show normal 3D specification and patterning. **c** shows 3D centralized and contacting the $1q^{111}$ quartet at the 56-cell stage (lateral). **d** shows $2a^{22}$–$2c^{22}$ contacting 3A–3C, whereas $2d^{22}$ does not at 56-cells (mid-vegetal). **e** shows 3D dividing before 3A–3C at the 72-cell stage (vegetal). **f**–**h** show identical stages in monensin-radialized development. **f** Shows a failure to centralize 3D. **g** shows that blastomeres of the 3Q and $2q^{22}$ quartets remain equivalent and the quartets are in contact at the 56-cell stage. **h** shows 3Q remaining undivided at 72-cells (vegetal). **c**, **e**, **f**, and **h** are photomicrographs of gallocyanin-stained embryos; **d** and **g** are camera lucida drawings. *cc* Cleavage cavity. Scale bar= 25 μm

perpendicular or else parallel to the plane of bilateral symmetry, each making contact with their associated 3A–3C macromeres, whereas $2d^{22}$ remains at the surface (Fig. 3d). 3D then divides before 3A–3C (Fig. 3e), producing a small 4D and large 4d in the 73-cell embryo. In radialized embryos, the transition to bilateral cleavage and the associated secondary axis were absent, as the $2q^2$ quartet divided in a radial pattern identical to $2a^2$–$2c^2$ (data not shown), and all four $2q^{22}$ micromeres extended into the cleavage cavity and contacted their associated 4Q macromeres, similar to $2a^{22}$–$2c^{22}$ in controls (Fig. 3g). The 3Q quartet remained undivided at the cell surface at the time of 3D division, similar to 3A–3C in controls (Fig. 3h).

Gastrulation in normal development is initiated in the late embryo and completed in the trochophore. Morphogenetic movements are bilaterally symmetric, with the vegetal region migrating along the B-quadrant midline to an anterior–ventral position beneath the prototroch (Fig. 4a–d). Swimming trochophores hatch from an egg chorion at 30 h and are active near the surface and throughout the water column. After gastrulation, adult anlagen, including dorsal shell field, lateral mantle, and ventral foot, become increasingly prominent, and the trochophore gives rise to the late trochophore, which integrates larval and adult structures (Fig. 4b; Fig. 6a–c). Gastrulation and differentiation in radialized larvae occurred in a quadri-radially symmetric pattern. A vegetal protuberance formed during the initial period of blastopore migration in controls and was gradually internalized at the vegetal pole (Fig. 4e,f,i–l). After internalization, the gut, perhaps the stomodeum and foregut, formed along a novel aboral–oral axis (Fig. 4g,h). Similar to radialized *P. vulgata* and *L. stagnalis* larvae, this axis ran parallel to the

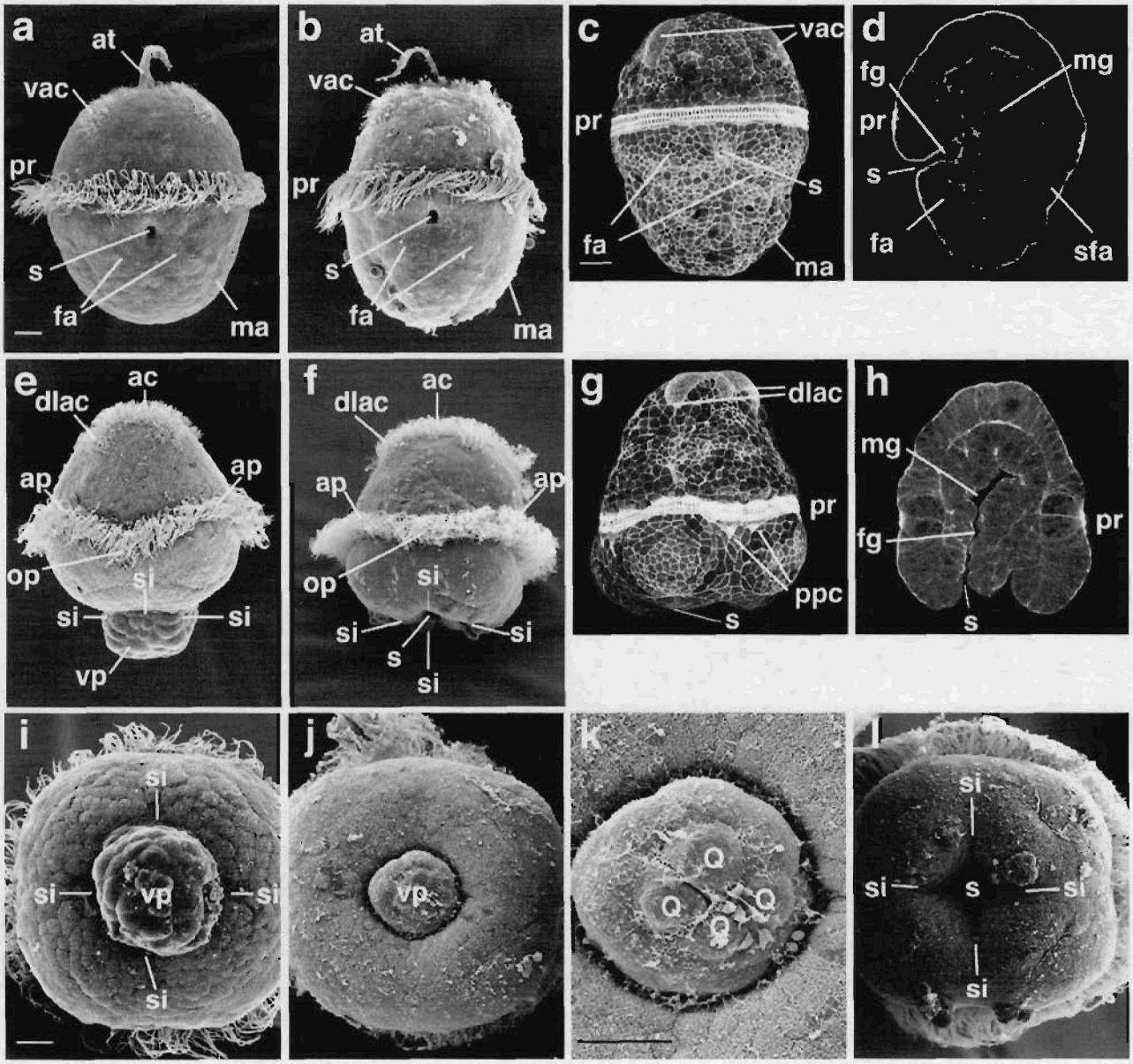

Fig. 4 Monensin-radialized *M. muscosa* trochophores undergo radial patterns of gastrulation and early differentiation. **a–d** show normal development. **a** and **b** show the normal completion of gastrulation at 37 h and early formation of the body plan at 48 h (ventral). **c** and **d** are a confocal projection and optical section of phalloidin-labeled actin in two larvae and show the organization of the gut about anterior–posterior and dorsal–ventral axes at 37 h (ventral and lateral). **e–l** show monensin-radialized development. **e** and **f** show protrusion of the vegetal pole at 37 h and its quadri-radial internalization at 48 h during gastrulation (lateral). **g** and **h** are a confocal projection and optical section of phalloidin-labeled actin in the same larva and show radial organization of the gut about the aboral–oral axis at 48 h (lateral). **i–l** show the sequence of protrusion (**i**) and quadri-radial internalization (**j–l**) of the vegetal pole during gastrulation at 37 (**i–k**) and 48 h (**l**; vegetal). **a**, **b**, **e**, **f**, **i**, **j** are scanning electron micrographs. *ac* Apical cilia, *ap* aboral prototroch peak, *at* apical tuft, *dlac* dorsal-like apical cilia arm, *fa* foot anlagen, *fg* foregut, *ma* mantle anlagen, *mg* midgut, *op* oral prototroch peak, *ppc* paired oral prototroch peak cell, *pr* prototroch, *Q* vegetal macromere, *s* stomodeum, *sfa* shell field anlagen, *si* stomodeal-like invagination, *vac* ventral apical cilia arm, *vp* vegetal protrusion. Scale bar=25 μm

original animal–vegetal axis, but was distinct from it due to gastrulation. Swimming larvae hatched 2 to 4 h later than controls and remained at the bottom (data not shown).

Patterns of differentiation were bilaterally symmetric in control larvae, arranged about the anterior–posterior and dorsal–ventral axes, but were quadri-radially symmetric in radialized larvae, arranged about the aboral–oral axis. Radialized larvae formed six distinct zones, each zone comprised two alternating quartets of quadri-radial patches; the two quartets offset from one another by 45° (Fig. 6d–i). Zone 1 at the aboral pole was formed by a field of apical cilia and zone 3 by the prototroch. Zone 6 at the oral pole

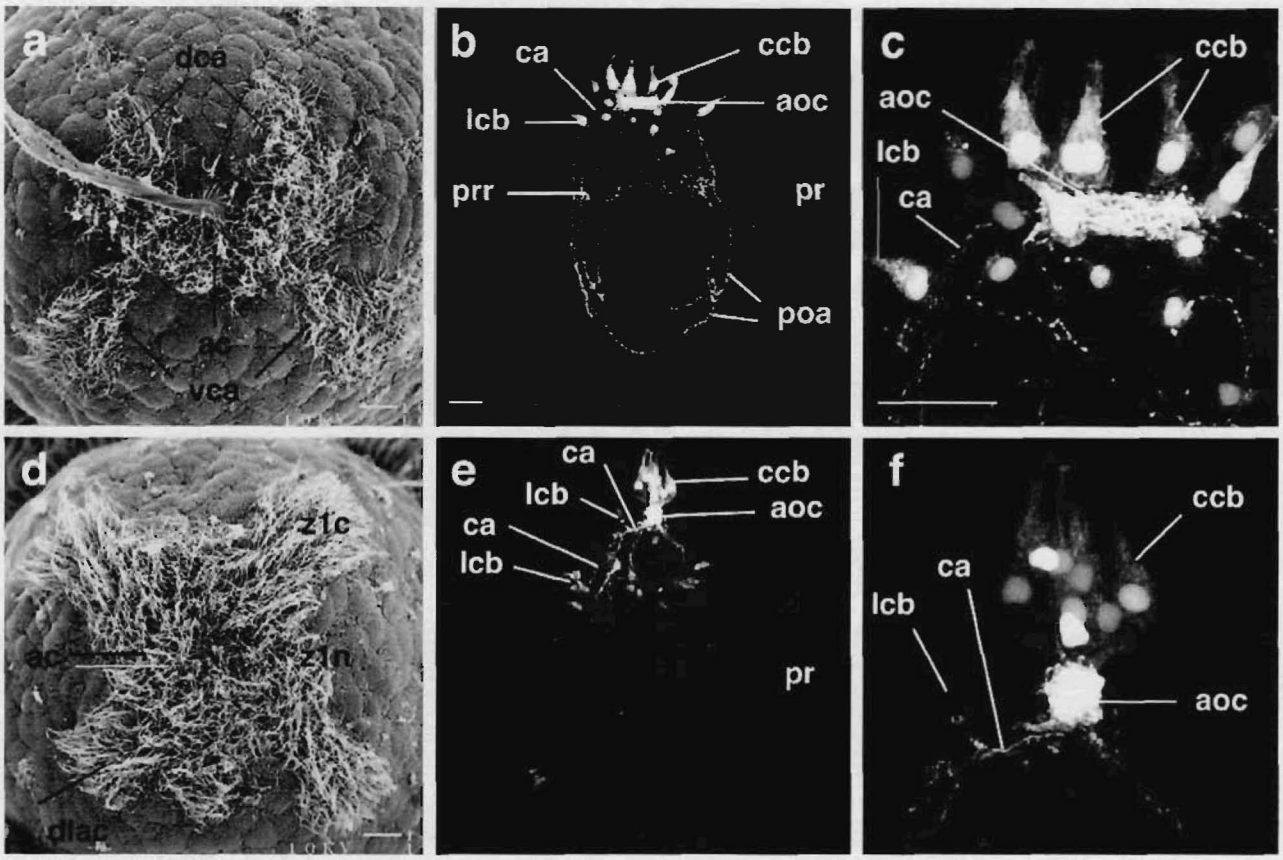

Fig. 5 Monensin-radialized *M. muscosa* trochophores lack an apical tuft but differentiate apical cilia and an apical organ in a radial pattern. **a**–**c** show normal development. **a** shows the apical tuft and surround apical cilia at 37 h (anterior). **b** and **c** are confocal micrographs of serotonergic-positive neurons and show the apical organ at 5 days (ventral). **d**–**f** show radial development. **d** shows the absence of an apical tuft but quadri-radially patterned apical cilia at 37 h (aboral). **e** and **f** are confocal micrographs of serotonergic-positive neurons and show radial differentiation of the apical organ but absence of trochal and post-trochal innervation at 5 days (lateral). **a** and **d** are scanning electron micrographs. *ac* Apical cilia, *aoc* apical organ/cerebral ganglion commissure, *dac* dorsal apical cilia arm, *dlac* dorsal-like apical cilia arm, *ca* connecting axon, *ccb* central cell body, *lac* lateral cell body, *pr* prototroch, *z1c* zone 1 ciliated arm, *z1n* zone 1 non-ciliated arm. Scale bar=25 μm

formed at the site of gastrulation and gave rise to a disorganized mix of potentially ectodermal and exogastrulated endodermal cells (Fig. 6g–i). Although distinct, the remaining zones could not be identified as corresponding to particular features of normal development (Fig. 6d).

Normal trochophores differentiate a long non-motile apical tuft and surrounding cilia, which form two long and angled ventral arms, two short and parallel dorsal arms, and a dorsal ciliary gap (Fig. 5a). Radialized larvae lacked an apical tuft but formed an expanded field of apical cilia at the aboral pole, with four short and perpendicular dorsal-like arms (Figs. 4e,f, 5d, 6d). In controls, serotonergic neurons of the apical organ and cerebral ganglia are present in controls beginning at 3 days (Fig. 5b,c). Dorsal-ventrally organized cell bodies, an anterior commissure, and paired neuronal tracts innervating the ventral and lateral aspects of the post-trochal trunk form, with central cell bodies residing directly on the commissure, whereas lateral cell bodies lie outside the commissure along axonal tracts. In radialized larvae, serotonergic neurons differentiated within zone 1 in a radial or quadri-radial, but never bilateral, pattern (Fig. 5e,f). Neurons formed the central and lateral cell bodies and apical commissures, but did not innervate the prototroch or post-trochal region. In controls, FMRF-amide-positive neurons are present in the anterior commissure with paired tracts running beneath the prototroch and projecting back into the post-trochal posterior region along paired lateral and ventral nerve cords (Fig. 7a,b). In radialized larvae, FMRF-amide-positive neurons differentiated in variable, non-bilateral patterns, forming apical commissures within zone 1 and with nerve cords/axonal tracts extending back into the post-trochal region (Fig. 7d). Control larvae form a circular muscle band beneath the prototroch at 3 days and an intricate network throughout the head and trunk region by 5 days (Fig. 7c). Radialized larvae formed circular muscle bands beneath the prototroch and a network of fibers in the shape of a pre-trochal radial basket and post-trochal radial bouquet (Fig. 7e). The prototroch (zone 3) in radialized

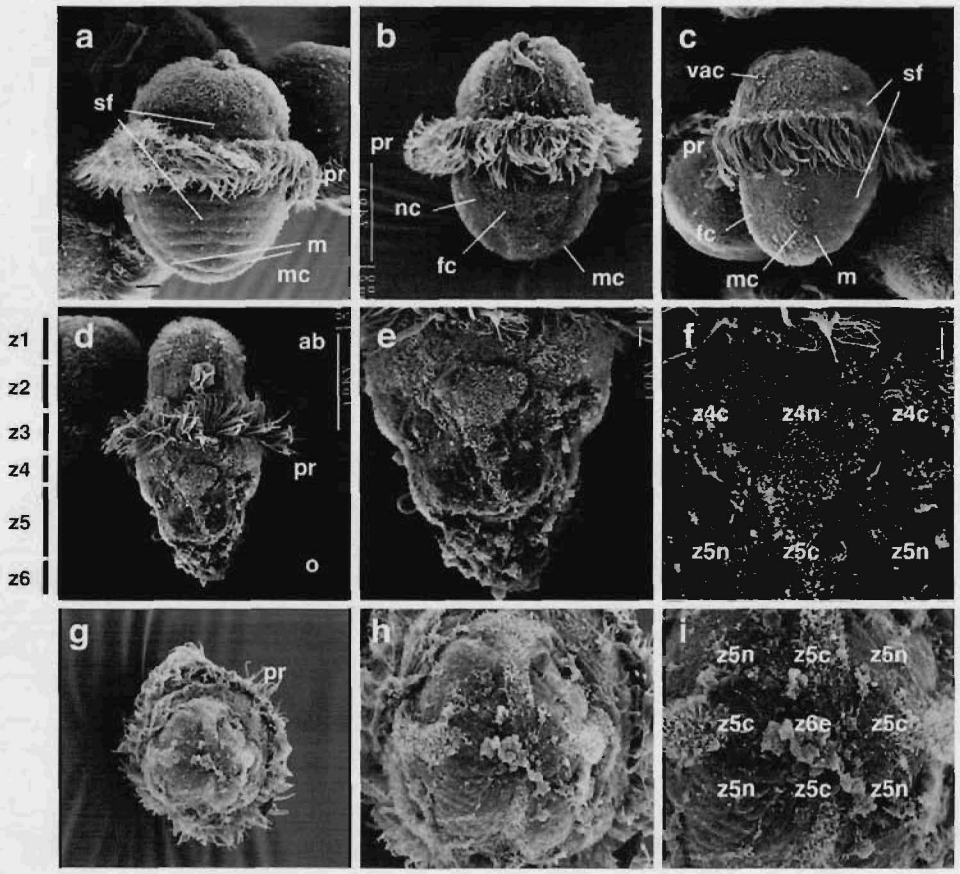

Fig. 6 Monensin-radialized *M. muscosa* late trochophores differentiate radial zones of cells or tissues along the aboral–oral axis. **a–c** are of normal development and show differentiation of adult structures about the anterior–posterior and dorsal–ventral axes at 4 days (dorsal, ventral, lateral, anterior–dorsal, posterior–dorsal, posterior–ventral). **d–i** are of monensin-radialized development and show the differentiation of two distinct quartets within each zone (z1–6) and global alignment of the different quartets into oral and aboral bands at 4 days (lateral and oral). **a–i** are scanning electron micrographs. *a* Anterior, *ab* aboral, *fc* foot cilia, *pr* prototroch, *m* mantle, *mc* mantle cilia, *nc* non-ciliated ventral region, *o* oral, *p* posterior, *pr* prototroch, *sf* shell field, *vac* ventral apical cilia, *z4c* zone 4 ciliated patch, *z4n* zone 4 non-ciliated patch, *z5c* zone 5 ciliated patch, *z5n* zone 5 non-ciliated patch, *z6e* zone 6 ectoderm/endoderm. Scale bar= 25 μm

larvae differentiated in a wave pattern of oral and aboral peaks rather than the normal flat ring (Fig. 4e). A pair of cells to either side of each oral peak exhibited a novel pattern of f-actin localization (Fig. 4c,g). Control trochophores form calcified epidermal spicules throughout the mantle edge (data not shown), whereas the shell field is uncalcified but regionalized into seven serially iterated plates (Fig. 6a). Calcified spicules were absent in radialized trochophores (data not shown) as were the shell plates (Fig. 6). In controls, short motile cilia cover the foot's ventral midline, and a lateral ciliary strip marks the mantle's outer edge, circumscribing the post-trochal region (Fig. 6b,c). It is unclear if mantle cilia are motile. In radialized larvae, zones 4 and 5 formed alternating sets of ciliated and non-ciliated quartets (Fig. 6d–i). Ciliated patches were motile, suggestive of active foot, or possibly mantle, cilia in controls. Paired post-trochal larval eyes, or ocelli, are present at 5 days in control larvae, but were absent in radialized ones (data not shown).

Monensin-induced radialization in the scaphopod *A. entalis*

To test the effect of monensin treatment on 3D activation and patterning in *A. entalis*, embryos were incubated in a 1-μM concentration for 3 h from the onset of the 24-cell stage, a period that extended through the transition to bilateral cleavage (Fig. 8a). Development was then assessed at later stages and compared to controls. After monensin treatment, larvae exhibited either radialized, abnormal, or normal development, with a mixture of all three present in approximately equal numbers in two separate experiments (Fig. 8b). An apical tuft, prototroch, dorsal shell and mantle, and ventral foot are present in normal 2-day veligers (Fig. 8c). At 5 days, the shell and mantle are extended around the body to meet along the ventral midline, with the foot now largely internal to the mantle and shell at the anterior end, and the pavilion forms as a small pocket at the posterior end (Fig. 8d). Monensin-radialized 1- to 2-day veligers exhibited a radial body plan with a truncated post-trochal region (Fig. 8e). The post-trochal region elongated in many older larvae and, although different tissues could not be clearly identified relative to normal development, an overall radialized appearance was maintained into the 3-day larval stage and beyond (Fig. 8f).

Discussion

Our results demonstrate that monensin and BFA provide simple, yet effective, experimental tools to inhibit the 3D

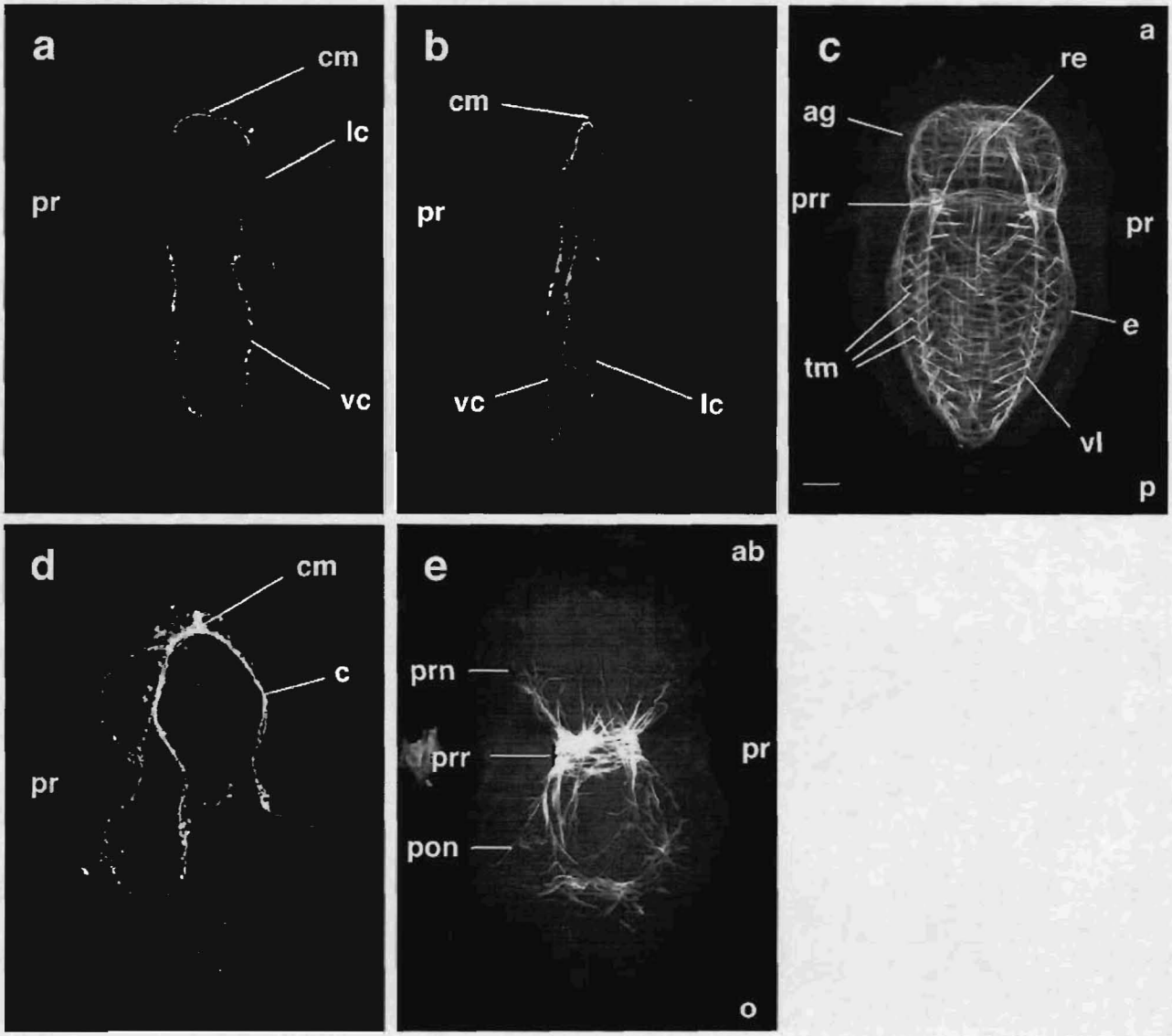

Fig. 7 *M. muscosa* monensin-radialized late trochophores differentiate muscle and nervous system tissues in a radial pattern. **a**–**c** are of normal development at 5 days. **a** and **b** are confocal projections of FMRF-amide-positive neurons and show tetraneuran nervous system symmetrically organized about the anterior–posterior and dorsal–ventral axes (dorsal and lateral). **c** is a confocal projection of phalloidin-labeled actin and shows a complex muscular network symmetrically organized about the anterior–posterior and dorsal–ventral axes (dorsal). **d** and **e** are of monensin-radialized development at 5 days. **d** is a confocal projection of FMRF-amide-positive neurons and shows variably formed nerve cords extending along the aboral–oral axis (lateral). **e** is a confocal projection of phalloidin-labeled actin and shows a complex muscular network radially organized about the aboral–oral axis (lateral). *ag* Apical grid, *c* FMRF-amide-positive nerve cord, *cm* FMRF-amide-positive cerebral commissure, *e* enrolling muscle, *lc* FMRF-amidic lateral nerve cord, *pon* post-trochal myofibril network, *pr* prototroch, *prn* pre-trochal myofibril network, *prr* prototroch ring muscle, *re* dorsal rectus muscle, *tm* transverse muscle, *vc* FMRF-amide-positive ventral nerve cord, *vl* ventrolateral longitudinal muscle. Scale bar=25 μm

organizer and radialize subsequent development in different molluscan clades and developmental systems. Given that the transition to bilateral symmetry is organizer-dependent for each of the three major clades tested (Cather and Verdonk 1979; Clement 1962; van den Biggelaar 1996), radialization in response to treatment suggests that both chemicals similarly inhibit, directly or indirectly, the organizer. In support of this, treatments made outside the window of organizer specification and patterning had minimal or no discernable effects in all three equal-cleaving species. In addition, although monensin and BFA act through distinct molecular or subcellular processes (Dinter and Berger 1998; Mayer 2003; Mollenhauer et al. 1990), they had seemingly identical effects on development in *P. vulgata*, suggesting that the observed phenotypes are not the result of a chemical-specific toxicity.

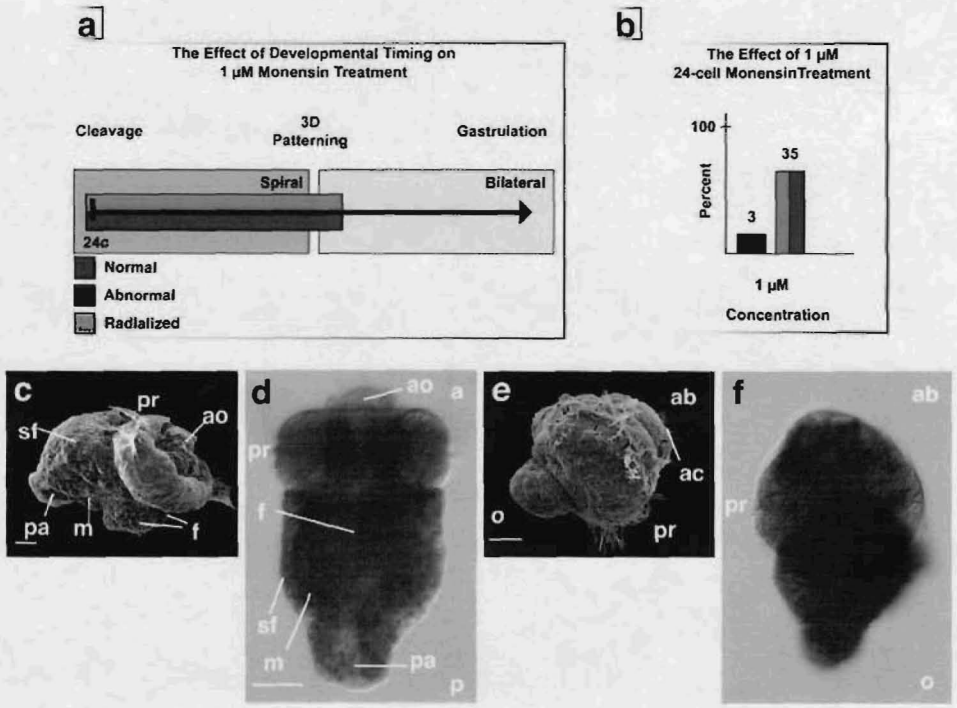

Fig. 8 Monensin treatment in *A. entalis* results in radialization of the body plan. **a** is a schematic showing the developmental timing of a 1 µM monensin treatment. **b** is a graph showing the effects of 1 µM monensin treatment. **c** and **d** show normal development with the body plan organized about the anterior–posterior and dorsal–ventral axes at 2 and 3 days (lateral and ventral). **e** and **f** show monensin-radialized development with the body plan organized about the aboral–oral axis at 2 and 3 days (lateral and lateral). *a* Anterior, *ao* apical organ, *f* foot, *m* mantle, *o* oral, *p* posterior, *pa* pavilion, *pr* prototroch, *sf* shell field. Scale bar=50 µm

Monensin and BFA radialization results in a similar loss of animal–vegetal extension in the three equal-cleaving species, indicating that radialization is similarly achieved through the inhibition of specification. This also suggests that the initially distinct actions of monensin and BFA converge downstream to inhibit the same developmental process, i.e., animal–vegetal extension. In *A. entalis*, the immediate developmental effects of monensin were not examined. Although specification is through determinant segregation by the polar lobe (Cather and Verdonk 1979; Wilson 1904), it is possible that, like polar-lobe-forming *C. fornicata*, animal–vegetal extension and contact also plays a role and was similarly blocked by treatment (Henry et al. 2006). Alternatively, monensin may have interfered with organizer activation or patterning rather than specification. The variable development of treated *A. entalis* embryos, ranging from normal to abnormal to radialized, might be attributed to the developmental asynchrony of normal development, as developmental timing is critical to radialization in the other species. It is not clear why BFA and not monensin radialized development in *L. stagnalis*. However, potentially lethal concentrations (10 µM) had no effect, suggesting that monensin was unable to diffuse across the egg capsule or vitelline membrane.

We found that organizer specification is different in equal-cleaving gastropods and polyplacophorans. In addition to previously noted differences in developmental timing (van den Biggelaar 1996; van den Biggelaar and Haszprunar 1996), *M. muscosa* extends a single non-cross-furrow 3Q macromere into the cleavage cavity, whereas *P. vulgata* and *L. stagnalis* extend all four, and, as described for the chiton *Acanthochiton crinitus*(van den Biggelaar 1996), 3D is always a non-cross-furrow macromere in *M. muscosa* but is a cross-furrow macromere in *P. vulgata* and *L. stagnalis*. These differences suggest that whereas some form of animal–vegetal extension and contact is generally conserved in equal-cleaving molluscs, the stochastic model of 3D specification (Arnolds et al. 1983), which requires that the 3Q macromeres be developmentally equivalent before contact and that there is a strong bias towards specifying a cross-furrow macromere as 3D, is gastropod-specific and does not apply to polyplacophorans. How a single non-cross-furrow macromere is initially specified to undergo extension and contact in *M. muscosa* is unknown. Further functional and molecular characterization of organizer specification in these and other equal-cleaving molluscs, including protobranch bivalves, will help clarify 3D's conservation and evolution in molluscs, as will similar characterizations in equal-cleaving clades of other phyla.

BFA- and monensin-radialized *P. vulgata* embryos in this study are similar to previous descriptions of monensin-radialized *P. vulgata* embryos (Kuhtreiber et al. 1988). Discrepancies arise at later stages; for instance, we did not observe quadri-radially arranged shell gland and stomodea invaginations, but these discrepancies may reflect differences in the larval stages examined and not actual differences in radialized development. It is unclear how BFA- and monensin-radialized development in different molluscs compares to UO126-radialized development in equal- and unequal-cleaving gastropods, including *P. vulgata*

(Lambert and Nagy 2001; Lambert and Nagy 2003; Lartillot et al. 2002b). For all three radialization techniques, there is a loss of bilateral cleavage in the embryo, indicating a similar inhibition of 3D's organizing activity. However, details of UO126-radialized larval development differ between studies of closely related taxa (Lambert and Nagy 2003; Lartillot et al. 2002b), and in all species outside of *M. muscosa*, gastrulation and the body plan remain largely undocumented. A more detailed analysis of BFA-, monensin-, and UO126-radialized development in a single species and across taxa is required to effectively compare the different species and techniques and, ultimately, to understand the organizing function of 3D.

The nature of the developmental axis established by organizer patterning and how it is translated into the body plan are poorly understood in spiral-cleaving lophotrochozoans. Although blastomere lineage contributions at the onset of gastrulation are stereotypic, they are not necessarily structure- or axis-specific (Dictus and Damen 1997), which suggests that, in many lineages, final decisions of developmental fate occur later during gastrulation, long after organizer patterning. In partial 2- and 4-cell embryos, only those lacking the D-quadrant blastomere fail to gastrulate (Wilson 1904). Thus, 3D might control downstream developmental fates by initiating gastrulation. However, our results in *M. muscosa* show that organizer patterning is not required for gastrulation, as radialized trochophores undergo quadri-radial patterns of morphogenetic movement. Instead, we found that the organizer-dependent developmental architecture, either bilateral or radial, at the onset of gastrulation predicts subsequent patterns of morphogenetic movement, differentiation, and the body plan. Thus, we propose that organizer patterning establishes a secondary developmental axis through its transformation of blastomere identities along the D-quadrant midline and that it does so in direct reference to subsequent patterns of gastrulation and only indirectly to the later body plan.

Developmental signaling centers pattern the early embryo and are required for proper establishment of the primary body axis in phyla as distant as chordates, cnidarians, and molluscs (Martindale 2005). In chordates and cnidarians, these organizing centers express similar sets of transcription factors and signaling molecules in the late embryo, through gastrulation, and into the adult body plan (Martindale 2005). In molluscs, patterning by the 3D organizer is completed before gastrulation (Cather and Verdonk 1979; Clement 1962), but similar sets of genes are expressed during gastrulation and into the body plan in lineages dependent upon 3D patterning (Lartillot et al. 2002a,b). This suggests, in conjunction with our own and other experimental studies, that the organizing function of 3D is only one part of a more general patterning network in gastrulation and may represent an ancient feature of early metazoan development. Genomic sequencing of now several spiral-cleaving lophotrochozoans, including the marine snail, *Lottia gigantea*, have recently become available and offer exciting new avenues for exploring the potential role of a developmental organizer in early animal evolution.

Acknowledgements We wish to thank A. Klerkx, L. Nederbragt, and A. van Loon for assistance in collecting and culturing *P. vulgata*, G. Zwaan for performing the experiments and initial analysis of *L. stagnalis*, L. Nederbragt, R. Rubicz, S. Santagata, and A. Wanninger for assistance in collecting, spawning, or fixing *M. muscosa*, and O. Lespinet for assistance in collecting and spawning *A. entalis*. We thank J. Priano and M. Rice for guidance and assistance with scanning electron micrographs, V. Foe, G. von Dassow, and others at the FHL NIH CCD for advice and the generous use of their confocal. We also thank D-H. Kuo, A. van Hook, K. O'Day, and D. Weisblat for their helpful comments and advice on earlier drafts of the manuscript. E. Gonzales wishes to thank M. Rice, B. Swalla, and D. Rokhsar for their guidance and support in the analysis and writing of this work. Finally, we greatly appreciate the kindness and support of staff and scientists at the University of Washington Friday Harbor Laboratories, the University of Paris VI Station Biologique de Roscoff, the Smithsonian Marine Station in Fort Pierce, the University of Göteberg Kristineberg Marine Station, the University of California at Berkeley Center for Integrative Genomics, and the University of Utrecht's former Department of Experimental Embryology. E. Gonzales was supported by NSF and Smithsonian predoctoral fellowships, two European Union Large Scale Facility grants, a Seaver Foundation grant to B. Swalla, and the NIH Genomics Training Grant to D. Rokhsar and the Center for Comparative Genomics.

References

Arnolds WJA (1979) Silver staining methods for the demarcation of superficial cell boundaries in whole mount embryos. Mikroskopie 35:202–206

Arnolds WJA, van den Biggelaar JAM, Verdonk NH (1983) Spatial aspects of cell interactions involved in the determination of dorsoventral polarity in equally cleaving gastropods and regulative abilities of their embryos, as studied by micromere deletions in *Lymnaea* and *Patella*. Roux's Arch Dev Biol 192:75–85

Cather JN, Verdonk NH (1979) Development of *Dentalium* following removal of D-quadrant blastomeres at successive cleavage stages. Wilhem Roux Arch Dev Biol 187:355–366

Clement AC (1952) Experimental studies on germinal localization in *Ilyanassa*: I. The role of the polar lobe in determination of the cleavage pattern and its influence in later development. J Exp Zool 121:593–624

Clement AC (1962) Development of *Ilyanassa* following removal of the D macromere at successive cleavage stages. J Exp Zool 149:193–216

Clement AC (1967) The embryonic value of the micromeres in *Ilyanassa obsoleta*, as determined by deletion experiments. I. The first quartet cells. J Exp Zool 166:77–88

Crampton HE (1896) Experimental studies on gastropod development. Wilhelm Roux' Arch Entwickl mech Org 3:1–19

Dictus WJAG, Damen P (1997) Cell lineage and clonal-contribution map of the trochophore larva of *Patella vulgata* (Mollusca). Mech Dev 62:213–226

Dinter A, Berger EG (1998) Golgi-disturbing agents. Histochem Cell Biol 109:571–590

Freeman G, Lundelius JW (1992) Evolutionary implications of the mode of D quadrant specification in coelomates with spiral cleavage. J Evol Biol 5:205–247

Halanych KM (2004) The new view of animal phylogeny. Annu Rev Ecol Evol Syst 35:229–256

Heath H (1899) The development of *Ischnochiton*. Zool Jahrb Abt Anat Ontog Tiere 12:567–656

Henry JQ, Perry KJ, Martindale MQ (2006) Cell specification and the role of the polar lobe in the gastropod mollusc *Crepidula fornicata*. Dev Biol 297:295–307

Kuhtreiber WM, van Til EH, van Dongen CAM (1988) Monensin interferes with the determination of the mesodermal cell line in embryos of *Patella vulgata*. Roux's Arch Dev Biol 197:10–18

Lambert JD, Nagy LM (2001) MAPK signaling by the D quadrant embryonic organizer of the mollusc *Ilyanassa obsoleta*. Development 128:45–56

Lambert JD, Nagy LM (2002) Asymmetric inheritance of centrosomally localized mRNAs during embryonic cleavages. Nature 420:682–686

Lambert JD, Nagy LM (2003) The MAPK cascade in equally cleaving spiralian embryos. Dev Biol 263:231–241

Lartillot N, Le Gouar M, Adoutte A (2002a) Expression patterns of fork head and goosecoid homologues in the mollusc *Patella vulgata* supports the ancestry of the anterior mesendoderm across Bilateria. Dev Genes Evol 212:551–561

Lartillot N, Lespinet O, Vervoort M, Adoutte A (2002b) Expression pattern of Brachyury in the mollusc *Patella vulgata* suggests a conserved role in the establishment of the AP axis in Bilateria. Development 129:1411–1421

Martindale MQ (2005) The evolution of metazoan axial properties. Nat Rev Genet 6:917–927

Mayer TU (2003) Chemical genetics: tailoring tools for cell biology. Trends Cell Biol 13:270–277

Mollenhauer HH, Morré DJ, Rowe LD (1990) Alteration of intracellular traffic by monensin: mechanism, specificity, and relationship to toxicity. Biochim Biophys Acta 1031:225–246

Sweet HC (1998) Specification of the first quartet micromeres in *Ilyanassa* involves inherited factors and position with respect to the inducing D macromere. Development 125:4033–4044

Tyler A (1930) Experimental production of double embryos in annelids and mollusks. J Exp Zool 57:347–407

van den Biggelaar JAM (1977) Development of dorsoventral polarity and mesentoblast determination in *Patella vulgata*. J Morphol 154:157–186

van den Biggelaar JAM (1996) Cleavage pattern and mesentoblast formation in *Acanthochiton crinitus* (Polyplacophora, Mollusca). Dev Biol 174:423–430

van den Biggelaar JAM, Guerrier P (1979) Dorsoventral polarity and mesentoblast determination as concomitant results of cellular interactions in the mollusk *Patella vulgata*. Dev Biol 68:462–471

van den Biggelaar JAM, Haszprunar G (1996) Cleavage patterns and mesentoblast formation in the Gastropoda: an evolutionary perspective. Evolution 50:1520–1540

Wanninger A, Haszprunar G (2002) Chiton myogenesis: perspectives for the development and evolution of larval and adult muscle systems in molluscs. J Morphol 251:103–113

Wilson EB (1892) The cell-lineage of *Nereis*. A contribution to the cytogeny of the annelid body. J Morphol 6:362–443

Wilson EB (1898) Considerations on cell-lineage and ancestral reminiscence based on a re-examination of some points in the early development of annelids and polyclads. Ann NY Acad Sci 11:1–28

Wilson EB (1904) Experimental studies in germinal localization. II. Experiments on the cleavage-mosaic in *Patella* and *Dentalium*. J Exp Zool 1:197–268